Inside the coupling of ladybird beetle elytra: elastic setae can facilitate swift deployment

Qiufeng Yuan [1, 2 †], Le Zong [3, 4 †], Jie Zhang [2], Jianing Wu [2], Yunqiang Yang [1, *], Siqin Ge [3,*]

1. School of Engineering and Technology, China University of Geosciences, Beijing, 100191, P. R. China
2. School of Aeronautics and Astronautics, Sun Yat-Sen University, Shenzhen, 518107, P. R. China
3. Institute of Zoology, Chinese Academy of Sciences, Beijing, 100101, China
4. University of Chinese Academy of Sciences, Beijing, 100049, China

† These authors contributed equally to this study.

*Corresponding author E-mail:

meyyq@cugb.edu.cn (Yunqiang Yang).

gesq@ioz.ac.cn (Siqin Ge).

ABSTRACT

The ladybird beetle (*Coccinella septempunctata*) is known for swift deployment of its elytra, an action that requires considerable power. However, actuation by thoracic muscles alone may be insufficient to deploy elytra at high speed because the maximum mechanical power that elytral muscles can produce is only 70% of that required for initiation of deployment. Nevertheless, the elytra open rapidly, within 3 ms in the initial phase, at a maximum angular velocity of 66.49 ± 21.29 rad s^{-1}, rivaling the strike velocity of antlion (*Myrmeleon crudelis*) mandibles (65 ± 21 rad s^{-1}). Here we hypothesize that elytra coupling may function as an energy storage mechanism that facilitates rapid opening by releasing elastic strain energy upon

deployment. To test this hypothesis and better understand the biomechanics of elytra deployment, we combined micro-computed tomography and scanning electron microscopy to examine the microstructure of the coupling of paired elytra. We found that two rows of setae on the internal edges of the elytra coupling structure undergo elastic deformation when the elytra are locked together. Kinematics observations and mathematical modelling suggest that the elastic potential energy stored in the compressed setae generates 40% of the power required for deployment of elytra. Our findings broaden insights into how ladybirds actuate elytra opening by a strategy of using both muscles and elastic microstructures, and demonstrate a distributed pattern of actuation that adapts to geometrical constraints in elytra locking.

KEY WORDS: Ladybird, Elytra coupling, Setae, Swift deployment

1. INTRODUCTION

Biological structures storing elastic energy for fast locomotion have been widely studied because of their diverse function (Farley et al., 1993), such as escaping from predators, catching prey, and self-righting (Bolmin et al., 2019; Henry et al., 2005; Ruan et al., 2020). Compared to storing energy in tendons or skeletal structures of vertebrates, some energy storage devices in invertebrates rely on elastic structures, for example, composite structures consisting of chitinized cuticle and the elastic protein resilin in limbs of locusts (*Schistocerca gregaria*) (Burrows and Sutton, 2012), and a pad of resilin in the thoraxes of fleas (*Archaeopsyllus erinacei*) (Sutton and Burrows, 2011). A flea is able to jump 150 times its body length by releasing a large amount of elastic energy stored in resilin (Koh et al., 2013). Another example of swift locomotion can be found in the appendages of ladybird beetles (*Coccinella septempunctata*). The elytra of ladybirds, transformed from the forewings to serve a protective function, cover and protect the fragile hindwings. The elytra are scoop-

shaped evaginations of the body integument attached by a membrane between the tergum and pleuron. The edge of the elytra is divided into three regions, namely the basal, costal, and sutural (medial) edges (Frantsevich, 2012b). At the sutural edge, the elytra can be locked together by a coupling structure consisting of a mortise and tenon, where the tenon is blade-shaped and inserts into the grooved mortise structure. When the elytra are closed, the apex of the elytra, where the basal and sutural edges converge, is in contact with the tergum and a small triangular scutellum. Prior to taking off, ladybirds can sequentially deploy their elytra and intricately folded hind wings within 100 ms (Baek et al., 2020; Saito et al., 2017; Saito and Okabe, 2015) (Movie 1). Conversely, in the locked state, the elytra can be tightly closed above the folded hindwings by locking structures located between elytra and thorax (Gorb and Embryology, 1998; Gorb, 1999).

Deployment of elytra in beetles is a fleeting event that seems to be actuated by a series of direct mesothoracic wing muscles (Dai and Yang, 2010; Frantsevich, 2011; GE et al., 2007). There is a consensus on the role of muscles that originate in front of the pleural ridge and insert into the anterior edge of the tergum or onto the basalare: they open the elytra together (Beutel and Haas, 2000a; Friedrich et al., 2006). Before deploying the elytra, the prothorax and the metathorax are pulled downward by the elytral muscles to release the elytra-locking structure, and then the elytra opens like a lever turning about the elytra-body articulation (Frantsevich, 2012b). Compared to hindwings, rapid deployment of the elytra may present a formidable challenge as the elytra are bulky and contain no elastic components, such as resilin (Song et al., 2020). Moreover, the elytral muscles are decentralized and part of the muscles are short or thin, and so they may be incapable of generating sufficient power to open the elytra (Hao and Du, 2018). Surprisingly, deployment of the elytra occurs within 100 ms, but the mechanism by which such speed is achieved remains unknow. In this combined experimental and theoretical study, we investigated the biomechanics of elytra opening powered by specialized structures coupling the two elytra together. We

quantify the mechanical power that elytral muscles can provide for deployment of elytra and assess whether that alone can account for their rapid unfolding, and investigate the role of microstructures embedded in the elytra coupling in their swift deployment.

2. MATERIALS AND METHODS

2.1 Animal samples

Thirty ladybirds (*Coccinella septempunctata*) were housed in an indoor terrarium at a temperature of 26°C and a humidity of 60% with a 12/12 h day/night cycle in Guangzhou, China (23.13°N, 113.27°E) (Fig. 1A). We weighed and averaged the masses of the elytra as m_e on a scale (Quintix35-1CN, Sartorius, Germany) (n = 20 ladybird samples). The width and length of each ladybird sample were measured using a vernier caliper (AIRAJ 1331, AIRAJ, USA) (Fig. 1B), and each living ladybird was measured three times. The body width a and length b were the maximum distance in the abdominal plane along the short and long axes of the body, respectively, as shown in Fig. 1B.

2.2 Elytra unfolding kinematics

To observe the kinematics of elytra unfolding, we used solid gum (PKTAK, Henkel, Germany) to attach the prothorax of ladybirds (n = 10) to a three-dimensional (3D)-printed fixed scaffold with a height of 5.30 cm (Fig. 1C). Then, a high-speed camera (Phantom, Micro CLY310, USA) equipped with a macro lens (Canon, EF100mmf/2.8LISUSM, Japan) was used to record kinematics of elytra deployment at 1000 fps, with elytra deployment being filmed twice for each ladybird (Fig. 1C). To quantify the kinematics of elytra opening, we defined a coordinate system with the scutellum at the origin o. The x axis originated at point o and extended posteriorly, with the z axis extending towards the abdomen, and the y axis oriented according to the right-hand rule. Elytra kinematics were measured from changes in the angle

between the elytra $\varphi(t)$, defined as the angle between the medial borders (sutural edges) of both elytra rotating about the elytra base on the abdominal plane, over a time t, thus defining the angular velocity $\omega(t)$ of elytra deployment (Fig. 1C). In order to elucidate the roles played by setae in elytra unfolding, some ladybirds (n = 5) were first anesthetized by freezing to reduce trauma and facilitate handling, followed by scraping off the setae inside the coupling structures on both elytra using a scalpel under a microscope (Olympus, CX33, Japan). After scraping, the insects were allowed to recover for a minimum of 30 min prior to filming, and we repeated the elytra unfolding experiments according to the procedures described above. In addition, we carried out control experiments that indicated that freezing anesthesia had no effect on speed of elytra opening.

To estimate the rotational kinetic energy E_r required for deploying the elytra at an angular velocity ω, a single elytron was modelled as a quarter of a spherical shell of mass m_e with a radius of R_1. The surface density of the elytra ρ was defined as $\rho = m_e / \pi R_1^2$. The moment of inertia J_{xp} with respect to an axis parallel to the x axis passing through the centroid was taken to be $J_{xp} = 5mR_1^2/3$ and the rotational kinetic energy E_r was defined as $E_r = J_{xp}\omega^2/2$.

2.3 Fixing setae in closed elytra

The shapes of setae, namely whether they were bent or remained straight when compressed, were visualized through a microscope (Olympus, CX33, Japan) and recorded by a camera (Canon, EOS 6D, Japan). We dropped superglue (Deli7146, Deli, China) onto the coupling structure of living ladybirds (n = 4 ladybirds), and closed the elytra tightly for 30 seconds to fix the setae when the two elytra were in contact. Then we held the posterior of the elytra with forceps under the microscope and gently pulled the closed elytra away in a direction perpendicular to the medial edge of the elytra. The shapes of the setae fixed by the glue were observed for each

elytron, and all were intact with no fracture or other damage, thus validating our procedure for processing elytra.

2.4 Scanning electron microscopy

Scanning electron microscopy (SEM) was used to examine the setae on the sutural edge of the elytra coupling. Each intact elytron (n = 6) dissected from three live ladybirds was cut into six sections with a scalpel. These fresh elytron samples (n = 36) were fixed by soaking in 2.5% glutaraldehyde at 26 °C for 3 h. We cleaned the samples three times with 0.1 mol L^{-1} phosphate buffer (pH = 7) for 20 min, and used a series of ethanol solutions between 75% and 100% at 5% intervals over 12 h to dehydrate the samples. Samples were processed for 15 h in a freeze-dryer (AlPHA 1-2 LDplus, Germany). Then they were coated with gold palladium (50 nm in depth) and mounted on SEM stubs with graphite adhesive tape, for observation under a SEM (FEI Quanta 200, Czech Republic) in high-vacuum mode at 15 kV (Zhang et al., 2020). From the SEM images, we counted the total number of the setae on elytra from each ladybird and measured the dimension of the setae along the x axis as described in Section 2.2.

2.5 Micro-computed tomography

To reconstruct the 3D configuration of the elytra and the thorax of the ladybirds, we used a Xradia MicroXCT-400 (Xradio Inc., California, USA). The samples (n = 4 ladybirds) were scanned at a voltage of 60 kV and a current of 133 μA. Ladybirds were mounted on a sample holder, and scanned with an axial resolution of 5 μm. The resulting data were then reconstructed using the software package Mimics (Materialise, Belgium) to discern elytral muscles and measure the gap between the coupled elytra.

2.6 Atomic force microscopy

Atomic force microscopy (AFM) was used to characterize mechanical properties of the setae. A piece of elytron with four setae (n = 5 ladybirds) was removed by using a scalpel under a microscope, and then placed horizontally on a glass slide (Fig. 1D and E). Then an AFM probe (RTESPA-150, BRUKER, USA) with a testing range of 50 MPa to 50 GPa was used with a Dimension Icon AFM (FastScan, BRUKER, USA) to measure the Young's modulus E of each setae (n = 20 elytron samples), which was tested at three points along its length. In peak force tapping mode, the vibrating tip applied a bending force at each point and recorded the movement of the seta. By real-time analysis of the force curves, the Young's modulus at each point was obtained and averaged by fitting with the Derjaguin, Muller, Toporov (DMT) model (Li et al., 2019; Zhang et al., 2021).

2.7 Measurement of coupling forces between elytra

For measuring the coupling force between elytra, we built an experimental platform consisting of a stepper motor and force sensor as shown in Fig. 1F (FUTEK, LSB200, USA). Living ladybirds were first anesthetized by freezing to eliminate muscle activity. Then each ladybird was mounted on the tip of a tapered plastic tube fixed on a slider that was driven by the stepper motor. We tested a total of five ladybirds, three times each. To make sure that the force applied on the coupling structure of the elytra was perpendicular to its edge, a string was glued with superglue (Deli7146, Deli, China) midway along the length of the right part of the coupled elytra, and the other end of the string was connected to a fixed force sensor. The sampling frequency of the sensor was set to 200 Hz. In each experiment, we separated the elytra by pulling on the string, and recorded the force F_c. The coupling force F_c applied to the coupling structure of the elytra was perpendicular, i.e., parallel to the pressure on the setae F. According to the tip displacement of the setae δ on the elytra coupling, the energy for

opening the elytra E_e by an external force was calculated as $E_e = F_c\delta$ (Dai et al., 2008).

2.8 Quantifying muscle power

Physiological cross-sectional area (PCSA) of a muscle is proportional to contractile force, while fascicle length reflects the length excursion of the muscle; both measures are used to determine how much work can be done by an individual muscle and how much power can be produced (Martin et al., 2020). Muscle volume V_m, fiber length L_m, and pennation angle γ (n = 4 muscle samples) were measured based on data obtained from digital 3D reconstructions. PCSA, which is a function of V_m, L_m, and ϕ, was expressed as $PCSA = V_m \cos\phi / L_m$ (Sellers et al., 2017). As values for maximum force (specific tension) in insect muscles are generally 5-35 N cm^{-2} and the maximum shortening velocity for insect muscles is on the order of 3-15 lengths s^{-1} (Josephson, 2009), we could obtain the maximum mechanical power P_m of muscles using the equation $P_m = PCSA \cdot T_s \cdot U_m$. Here, T_s is the muscle specific tension, and U_m is the speed of muscle shorting.

2.9 Mathematical modelling of energy storage in setae

To analyse effects of compressed setae on the kinematics of elytra opening, we built a mathematical model. As shown in Fig. 1G, using the elastic cantilever model, a single seta with a length of L_s and a constant radius R_s was treated as an oblique beam oriented at an angle θ to the horizontal line (Autumn et al., 2006). When a ladybird closed its elytra, the setae on one elytron were compressed by the other elytron. This caused a maximum bending deformation δ of each seta in the same direction. We decomposed the force F bending the setae into tangential F_t and normal components

F_n that were parallel and perpendicular to the setae, respectively. In this bending problem, only the latter force, i.e., F_n, influenced deformation of the seta. The normal stiffness K_n was measured using $K_n = 3IE / L_s^3$, in which I was the area moment of inertia calculated as $I = \pi R_s^4 / 4$. We calculated the elastic potential energy stored in the compressed setae as follows (Bullock and Federle, 2009).

$$E_s = n \int \frac{3\pi R_s^4 E \delta}{4 L_s^3 \cos^2 \theta} \mathrm{d}\delta \quad (1)$$

The number *n* of setae and their geometry were measured from SEM images. Tip displacement δ of setae was defined to be equal to the difference between the height of the seta and the gap between the coupled elytra. Then, the power available from the elastic potential energy P_s was obtained by $P_s = E_s / t$.

3. RESULTS

3.1 Kinematics of elytra unfolding

Using a high-speed camera, we closly observed elytra opening in a living ladybird (*Coccinella septempunctata*) with intact elytra (Fig. 2A). During elytra deploying, a crevice of length L_c (*t*) formed over a time *t*, starting from 0 mm and ultimately extending to the full length of the coupling, namely, L_e = 5.5 mm (*n* = 10 ladybird samples) (Fig. 2B). The elytra kinematics were identified by measuring the crevice angle of the elytra $\varphi(t)$ with respect to the duration *t*, defined as the angle between the medial borders (sutural edges) of the two elytra rotating about the elytra base on the abdominal plane, from which the angular velocity $\omega(t)$ of elytra deployment could be calculated. Using the region-wise mapping of angular velocity shown in Fig.

2C, the entire process of elytra deployment could be categorized into three phases, namely the initial, middle and final phases. At the end of the initial phase of elytra deployment at t = 3 ms, the crevice split rapidly to L_c (3) = 5.01 ± 0.12 mm = (91.09 ± 2)% L_e (n = 10 ladybird samples), which suggested that the elytra were fully unlocked at φ (3) = 10.03 ± 0.94 deg. (n = 10 ladybird samples), and the average angular velocity in the initial phase was ω_1 = 3.81 ± 1.22 deg. ms^{-1}. However, in the middle phase, the ladybird required an additional 12 ms to deploy the elytra to φ (15) = 20.47 ± 1.87 deg. (n = 10 ladybird samples). The angular velocity on average during this phase exhibited the lowest value among the three phases as ω_2 = 0.93 ± 0.31 deg. ms^{-1}, only 1/4 that of the initial phase (Movie 1). The final phase had an average angular velocity of ω_3 = 1.92 ± 0.73 deg. ms^{-1}, which was only 50% of the initial angular velocity.

Such rapid movement requires high energy over a short time, but the mechanism of generating this energy remains unknown. Deployment of elytra may be actuated through movement of the hinged-base of elytra driven by a limited number of direct and/or indirect elytral muscles (Frantsevich et al., 2005). Therefore, we examined the musculature involved in elytra deployment using micro-CT-scanning to determine whether the swift deployment of elytra can indeed be powered by these elytral muscles alone.

3.2 Micro-computed tomography of elytral muscles

The opening and closing of elytra have been previously ascribed to intrinsic muscles attached to the tergite and pleurite (Frantsevich, 2012b). Here we use the muscle numbering principle based on anatomical characterization of the muscles and the elytral pivot (Beutel and Haas, 2000b; Larsén, 1966). Specifically, elytra deployment is actuated mainly by a combination of M. 40 (M. mesonoti secundus), M. 47 (M. noto-pleuralis), M. 50 (M. episternosternalis), and M. 60 (M. noto-coxalis), which are

the muscles in the mesothorax of a ladybird that abduct, elevate, and extend the elytra (Fig. 3, Movie 2). The functions of M. 40 and M. 47 are to release elytral fixation (antagonist of M. 39) and the elytral base (depressor of the lateral notum), respectively. Previous descriptions suggestions that muscle M. 60, which is well developed, may be the main muscle for actuating elytra opening (GE et al., 2007). We scanned ladybird thorax morphology, especially the musculature of the mesothorax, by digital 3D micro-computed tomography, and as shown in Figs. 3A-D, the physiological cross-sectional area (PCSA) of M. 60 could be calculated by measuring muscle volume, fiber length, and pennation angle. The pennation angle has a negligible effect on the PCSA calculation, as shown in Figs. 3B and 3D, M. 60 may be the parallel-fibered muscle that shortens along the long axis of the fiber bundle when the muscle contracts (Martin et al., 2020). Therefore, PCSA = (0.16 ± 0.01) × 10^5 μm^2 (n = 4 muscle samples), and the maximum power output by M. 60 was P_m = 0.028 ± 0.002 μJ ms^{-1} (700 W kg^{-1}) (n = 4 muscle samples), similar to the power output of fast insect muscle (500 W kg^{-1}) (Josephson, 1993; Josephson et al., 2001). Take into account average angular velocity of elytra opening in the initial phase, average body size R_1 = 2.59 ± 0.20 mm, and body mass m_e = 5.02 ± 0.23 mg (n = 20 ladybird samples), the rotational kinetic energy for elytra deployment in the initial phase was E_r = 0.11 ± 0.06 μJ with a power of P_e = 0.04 ± 0.02 μJ ms^{-1}. Therefore, the elytral muscles cannot produce sufficient power for opening elytra at the observed high speed because muscle power $P_m = 70\% P_e$ (Fig. 3E). In this case, ladybirds must rely on another source of power, such as elastic energy stored in the elytra. So, we combined micro-CT and SEM imaging to further examine elytra coupling.

3.3 Effects of setae on elytra unfolding

We initially reconstructed the ladybird's elytra coupling through micro-CT imaging (Fig. 4A) and identified the tenon and mortise structures (Frantsevich, 2012a). The tenon structure is blade-shaped and inserts into the grooved mortise structure (Fig. 4B, C). SEM images showed that the length and height of the tenon were $L_t = 5.20 \pm 0.03$ mm and $H_t = 44.51 \pm 0.02$ μm (n = 6 elytron samples), respectively (see Section 2.4). The mortise and the tenon unlock during rapid deployment of the elytra, as shown in the schematics of Fig. 5A. At the end of the initial phase, the length of the crevice arrived at $L_c(3) = 96.71\% L_t$ at a splitting angle of $\varphi(3) = 10$ deg. Moreover, the gap between the tenon blade and mortise groove $G_0 = 55.82 \pm 5.24$ μm (n = 6 elytron samples), was greater than H_t (Fig. 5B, C), indicating that the entire coupling structure uncoupled completely by the end of the initial phase.

Notably, the SEM images showed that two rows of setae were distributed along the internal edge of the elytra coupling, namely the upper edge of the blade of the tenon, and the upper edge of the ventral ridge of the mortise (Figs. 4B, C). These setae were distributed evenly along both elytra, with 126 ± 20 (n = 6 elytron samples) on each. The setae had tubular basal parts and pointed tips, and radiated toward the opposite part of the coupling structure at an angle θ (Fig. 4D). Along the x axis, the length of the setae L_s increased from 24.77 ± 2.83 μm to 56.25 ± 3.31 μm (n = 36 elytron samples), illustrating that the setae became longer posteriorly from the scutellum (Fig. 5D). Specifically, L_s in the proximal section of the elytra, between 0 and 5.2 mm from the scutellum, fluctuated around 28.57 ± 2.28 μm. By contrast, L_s at locations between 5.2 mm and 6.4 mm from the scutellum (distal section of the elytra) rose from 28.95 ± 1.62 μm to 56.25 ± 3.31 μm. The angle θ varied similarly, increasing from 27.20 ± 0.46 deg. to 51.88 ± 0.79 deg. (n = 36 elytron samples). To determine the configuration of setae inside a pair of coupled elytra, we measured the

gap within the coupling structure H_2 from micro-CT images. The gap H_2 remained relatively stable at 0 - 5.2 mm from the scutellum, and then rose from 7.44 ± 1.82 μm to 11.59 ± 0.79 μm (n = 4 ladybird samples) in the distal section of the elytra (Fig. 5E). Along the x axis, the gap H_2 in the coupling structure was always smaller than the length of the setae $H_1 = L_s \sin\theta$, indicating that setae are forced to bend by the internal surface of the coupling structure when the elytra are coupled. To further explore the shape of the setae in the closed elytra, we developed a technique by which the setae in the closed position of elytra were fixed by glue (see Section 2.3). Fig. 5E shows deflection of setae in the fixed samples, verifying that the setae are bent in the closed elytra coupling structure. These observations suggested that elastic energy stored in the compressed setae may contribute to swift opening of elytra in their initial phase of deployment.

In order to elucidate the roles played by setae in elytra unfolding, living ladybirds in which all the setae inside the elytra coupling had been scraped off were filmed at a frame rate of 1000 fps. Fig. 6 shows typical events and corresponding kinematics of elytra deployment in the absence of setae. During the initial phase of elytra opening, average angular velocity was 0.79 ± 0.05 deg. ms^{-1} (n = 5), which was only 1/5 that for elytra with setae, consistent with setae compression contributing to more rapid elytra deployment in the initial phase (Movie 3).

3.5 Elytra unfolding facilitated by setae

We built a mathematical model to evaluate the impact of compressed setae on elytra deployment. AFM measurements (see Section 2.6) showed that the Young's modulus of the setae was E = 300 MPa. When the elytra were coupled together, a load F perpendicular to the substrate was applied to the tip of each seta (Fig. 1G). SEM imaging showed that the average normal displacement was $\bar{\delta} = H_1 - H_2 = 10.36 \pm 0.88$ μm, and the setae had an average length $\bar{L}$ = 28.56 ± 2.27 μm and angle $\bar{\theta}$ =

38.38 ± 2.22 deg. The average elastic potential energy stored in the compressed setae was calculated as $E_s = 4.27 \times 10^{-2}$ μJ, with the power available from the elastic potential energy being $P_s = 1.42 \times 10^{-2}$ μJ ms^{-1}. Mathematical modelling suggested that setae release provides 38.9% of the rotational kinetic energy E_r of elytra deployment, supplying 35.6% its power P_e. Therefore, the energy stored in setae may play an essential role in swift deployment of the elytra.

We can derive the elastic energy E_s for setae of different lengths L_s and angles θ based on the theory proposed in Section 2.9. Fig. 7A shows that E_s increases with θ, but decreases with L_s for setae of constant radius, so that stored elastic energy is greater in shorter setae deflected by a higher angle (yellow regions in Fig. 7A) and is reduced in longer setae at lower angles (blue regions). For a given θ, E_s reaches a maximum for L_s between 30 and 35 μm, consistent with the actual length of setae (indicated by the region outlined in orange). Since beam buckling may occur when θ turns more than 60 deg., we only consider deflection angles smaller than this critical value. For constant L_s, E_s reaches a maximum at θ = 60 deg.; however, excessive elastic energy storage may break the elytra-to-body interlocking. The average coupling force of elytra was measured to be F_c = 16.50 ± 0.25 mN, thus the critical energy required for opening the elytra by an external force can be estimated as $E_e = F_c\delta = 0.17$ μJ (Fig. 7B). Fig.7B clarifies that when θ > 54 deg., the elastic energy of setae (actual L_s = 30 μm) reaches $E_s = 0.16$ μJ ≈ E_e (purple horizontal line in Fig. 7B), which suggests that under these conditions, the elytra may lose ability to close tightly. When θ becomes smaller than 35 deg., E_s = 2.54×10^{-2} μJ, which is only 23% of the rotational kinetic energy of elytra E_r, uncovering that E_s is in that

case insufficient for swift elytra deployment. Thus, the effective range of the setae angle θ lies between 35 and 54 deg., indicated by the pink shaded area in Fig. 7B, and consistent with anatomical microstructure corresponding to the region outlined in red in Fig. 7A. Therefore, the optimized length and angle are organized as 30 μm and 54 deg. respectively, consistent with postmortem examination and indicated by the region in Fig. 7A outlined in both red and orange, which suggests a trade-off for ladybirds between swiftness of elytra opening and stability of elytra locking.

4. DISCUSSION

The unfolding kinematics of elytra have revealed three phases that are characterized by different angular velocities. The initial phase is the most energetically challenging as the tightly locked elytra have to be unlocked, and the energy required to open them may be much higher than during the following phases (Frantsevich, 2012a). Surprisingly the insect generates an ultra-fast deployment with a maximum angular velocity in the initial phase that is four times that of subsequent phases, comparable to that of the ant lion's (*Myrmeleon crudelis*) mouthparts in a strike (Lambert et al., 2011). To explore how this enormous energy is produced, we examined the musculature involved in elytra deployment. Muscles produce a broad range of motions in living animals. Some of the most powerful and rapid movements occur during locomotor behaviors such as flying and leaping, and this power is usually generated by muscle contraction (Camp et al., 2015). However, quantification of the power output of elytral muscles suggests that they are insufficient to produce sufficient the power for opening elytra at such high speed. Thus, ladybirds may also utilize a less apparent actuation mechanism. To overcome the energetic limitations of muscle contraction when on propelling both swift and powerful locomotion, many insects use elastic structures that can store energy (Burrows et al., 2008; Burrows, 2003; Wan et al., 2016). For instance, during take-off, locusts (*Schistocerca gregaria*)

very rapidly accelerate to an initial speed of 3 m s^{-1} in 30 ms through releasing energy stored in two bow-shaped semi-lunar processes at the femorotibial joint (Cofer et al., 2010). The champion jumpers in nature, namely froghoppers (*Philaenus spumarius*), can jump at a velocity of 4 m s^{-1} by releasing energy stored in a strengthened thoracic cuticle (Burrows, 2003). To explore whether ladybirds utilize the same strategy, the elytra coupling structure was closely examined. We found that setae on the internal edge of the elytra coupling structure store energy by functioning as springs, and play an important role in rapid elytra movement during the initial phase of deployment. These setae are evenly distributed along the elytra coupling, and become longer posteriorly from the scutellum. Since elytra gradually unfold from more posterior positions, the increases in both the size of the gap between elytra and the length of setae may serve to maintain deformation of the setae across the entire interdigitated suture. Our mathematical model explains the effect of seta length and angle on energy storage capacity of setae and the tightness of elytra locking, showing that the setae are characterized by lengths and angles that may represent a trade-off for ladybirds between swiftness of elytra opening and stability of elytra locking.

Compared with locusts or froghoppers that release concentrated energy through a single elastic structure, the distributed actuation pattern in ladybirds that stores energy in setae evenly distributed along each elytron has the advantages of both morphological feasibility and functional adaptation. In order to further consider potential mechanical advantages of coupling elytra through linear arrays of setae, we examine the following scenarios involving a single seta. (1) Assuming that a ladybird stored energy for elytra deployment in only one 30 μm-long seta at an angle of 50 deg., it would have to be 21.59 μm in diameter, four times the measured value, to store the same amount of energy as evenly distributed 5.5 μm-diameter setae. Furthermore, a 21.59 μm-long seta would not fit in the coupling gap H_2, which is only 11.59 μm wide when the coupling structure is fully interlocked. (2) Alternatively, energy could be stored in one seta of diameter 5.5 μm at the experimentally measured

angle of 39 deg. The length of the seta L_s would then have to be 4.80 μm, only 1/6 of the actual value. In this case, the seta would undergo no bending because the height of the seta H_1 would be smaller than H_2, so the seta in the closed elytra would not be able to store energy. (3) Most of the morphological adaptations for energy storage in insects are composite structures consisting of resilin and chitinous cuticle (Burrows et al., 2008). Hard materials (chitinous cuticle) can store more energy under less deformation but are liable to fracture, whereas elastic materials (resilin) can prevent fracture during bending or other distortion of the hard cuticle (Burrows and Sutton, 2012). Given the requirement for stable coupling of the elytra when closed and sufficient energy storage for deployment upon opening, and assuming energy storage in a seta of the same dimensions as that measured experimentally, the Young's modulus of a single seta would have to be 60 GPa (c.f. 0.3 GPa xperimentally), close to that of aluminum (68 GPa), which would result in the seta fracturing as it is bent during elytra closing.

In addition, this distributed actuation pattern allows for more gradual stable energy release, which may help to alleviate damage to the muscles involved in fast movements of the dome-like shell (Dai and Guan, 2012; Hu et al., 2018). Furthermore, since beetle flight muscles that actuate the high-frequency vibration of hindwings are well developed and kinematically complicated, using elastic energy stored in setae to open elytra may not require a large number of muscles, which may provide additional space for flight muscles (Haas and Beutel, 2001; Josephson et al., 2000). This specifically distributed-actuation pattern along a ladybird's elytra may inspire the next-generation lightweight origami capable of fast and efficient deployment.

Acknowledgements

We thank Dr. Li Gong from Instrumental Analysis & Research Center of Sun Yat-sen University for the assistance in measuring the Young's modulus of elytra. We thank Dr. Leonid Frantsevich from the Schmalhausen-Institute of Zoology (UkrNAS) for his valuable comments on the experimental part. We sincerely thank Dr. Hamed Rajabi from London South Bank University for his comments on the experiments and revision of the draft. We thank Caixia Gao and Xiaowei Qin from Institute of Zoology, Chinese Academy of Sciences, for CT scan and freeze-drying.

Competing interests

We declare we have no competing interests.

Author contributions

J.W, Y.Y, and S.G conceived the project. Q.Y, L.Z, and J.Z planned and carried out the experiments. Q.Y and L.Z participated in data analysis. Q.Y and J.Z built the mathematical model. J.W, and Q.Y wrote the manuscript.

Funding

This work was supported by the National Natural Science Foundation of China (grant No. 51905556), the Grant for Popularization of Scientific and Technological Innovation of Guangdong Province (grant No. 2020A1414040007), the research grant of Sun Yat-sen University for Bairen Plan (grant No. 76200-18841223), and Shenzhen Science and Technology Innovation Program (Grant No. GXWD20201231165807008, No. GXWD 20200830220051001).

References

Autumn, K., Majidi, C., Groff, R. E., Dittmore, A. and Fearing, R. (2006). Effective elastic modulus of isolated gecko setal arrays. *J Exp Biol* **209**, 3558-68.

Baek, S.-M., Yim, S., Chae, S.-H., Lee, D.-Y. and Cho, K.-J. (2020). Ladybird beetle–inspired compliant origami. *Science Robotics* **5**.

Beutel, R. G. and Haas, F. (2000a). Phylogenetic relationships of the suborders of Coleoptera (Insecta). Cladistics 16, 103-141.

Beutel, R. G. and Haas, F. J. C. (2000b). Phylogenetic relationships of the suborders of Coleoptera (Insecta). **16**, 103-141.

Bolmin, O., Wei, L., Hazel, A. M., Dunn, A. C., Wissa, A. and Alleyne, M. (2019). Latching of the click beetle (Coleoptera: Elateridae) thoracic hinge enabled by the morphology and mechanics of conformal structures. *J Exp Biol* **222**, jeb196683.

Bullock, J. M. and Federle, W. J. J. o. E. B. (2009). Division of labour and sex differences between fibrillar, tarsal adhesive pads in beetles: effective elastic modulus and attachment performance. **212**, 1876-1888.

Burrows, M., Shaw, S. R. and Sutton, G. P. J. B. b. (2008). Resilin and chitinous cuticle form a composite structure for energy storage in jumping by froghopper insects. **6**, 1-16.

Burrows, M. and Sutton, G. P. J. J. o. E. B. (2012). Locusts use a composite of resilin and hard cuticle as an energy store for jumping and kicking. **215**, 3501-3512.

Burrows, M. J. N. (2003). Froghopper insects leap to new heights. **424**, 509-509.

Camp, A. L., Roberts, T. J. and Brainerd, E. L. (2015). Swimming muscles power suction feeding in largemouth bass. *Proc Natl Acad Sci U S A* **112**, 8690-5.

Cofer, D., Cymbalyuk, G., Heitler, W. and Edwards, D. J. J. o. E. B. (2010). Neuromechanical simulation of the locust jump. **213**, 1060-1068.

Dai, L. and Guan, F. L. (2012). Design and Manufacture of Double-Ring Deployable Truss. In *Advanced Materials Research*, vol. 566, pp. 357-360: Trans Tech Publ.

Dai, Z. and Yang, Z. J. J. o. B. E. (2010). Macro-/micro-structures of elytra, mechanical properties of the biomaterial and the coupling strength between elytra in beetles. **7**, 6-12.

Dai, Z., Zhang, Y., Liang, X. and Sun, J. (2008). Coupling between elytra of some beetles: mechanism, forces and effect of surface texture. *Sci China C Life Sci* **51**, 894-901.

Farley, C. T., Glasheen, J. and McMahon, T. A. (1993). Running springs: speed and animal size. *J Exp Biol* **185**, 71-86.

Frantsevich, L. (2012a). Double rotation of the opening (closing) elytra in beetles (Coleoptera). *Journal of insect physiology* **58**, 24-34.

Frantsevich, L. (2012b). Experimental evidence on actuation and performance of the elytron-to-body articulation in a diving beetle, Cybister laterimarginalis (Coleoptera, Dytiscidae). *Journal of insect physiology* **58**, 1650-1662.

Frantsevich, L., Dai, Z., Wang, W. Y. and Zhang, Y. J. J. o. E. B. (2005). Geometry of elytra opening and closing in some beetles (Coleoptera, Polyphaga). **208**, 3145-3158.

Frantsevich, L. J. J. o. B. E. (2011). Mechanisms modeling the double rotation of the elytra in beetles (Coleoptera). **8**, 395-405.

Friedrich, F., Beutel, R. J. J. o. Z. S. and Research, E. (2006). The pterothoracic skeletomuscular system of Scirtoidea (Coleoptera: Polyphaga) and its implications for the high‐level phylogeny of beetles. **44**, 290-315.

GE, S. Q., Beutel, R. G. and YANG, X. K. J. S. E. (2007). Thoracic morphology of adults of Derodontidae and Nosodendridae and its phylogenetic implications (Coleoptera). **32**, 635-667.

Gorb, S. N. J. I. J. o. I. M. and Embryology. (1998). Frictional surfaces of the elytra-to-body arresting mechanism in tenebrionid beetles (Coleoptera: Tenebrionidae): design of co-opted fields of microtrichia and cuticle ultrastructure. **27**, 205-225.

Gorb, S. N. J. J. o. M. (1999). Ultrastructure of the thoracic dorso‐medial field (TDM) in the elytra‐to‐body arresting mechanism in Tenebrionid Beetles (Coleoptera: Tenebrionidae). **240**, 101-113.

Haas, F. and Beutel, R. G. J. Z. (2001). Wing folding and the functional morphology of the wing base in Coleoptera. **104**, 123-141.

Hao, P. and Du, J. J. J. o. M. S. (2018). Mechanical properties of bio-mimetic energy-absorbing materials under impact loading. **53**, 3189-3197.

Henry, H. T., Ellerby, D. J. and Marsh, R. L. (2005). Performance of guinea fowl Numida meleagris during jumping requires storage and release of elastic energy. *J Exp Biol* **208**, 3293-302.

Hu, F., Song, Y., Huang, Z., Liu, W. and Li, W. J. A. A. (2018). Malleability and optimization of tetrahedral metamorphic element for deployable truss antenna reflector. **8**, 055217.

Josephson, R. (1993). Contraction dynamics and power output of skeletal muscle. *Annual review of physiology* **55**, 527-546.

Josephson, R. (2009). Muscle System. In *Encyclopedia of Insects*, pp. 675-680: Elsevier.

Josephson, R. K., Malamud, J. G. and Stokes, D. R. (2001). The efficiency of an asynchronous flight muscle from a beetle. *J Exp Biol* **204**, 4125-4139.

Josephson, R. K., Malamud, J. G. and Stokes, D. R. J. J. o. E. B. (2000). Power output by an asynchronous flight muscle from a beetle. **203**, 2667-2689.

Koh, J.-S., Jung, S.-P., Noh, M., Kim, S.-W. and Cho, K.-J. (2013). Flea inspired catapult mechanism with active energy storage and release for small scale jumping robot. In *2013 IEEE International Conference on Robotics and Automation*, pp. 26-31: IEEE.

Lambert, E. P., Motta, P. J. and Lowry, D. (2011). Modulation in the feeding prey capture of the ant‐lion, Myrmeleon crudelis. *Journal of Experimental Zoology Part A: Ecological Genetics and Physiology* **315**, 602-609.

Larsén, O. (1966). On the morphology and function of the locomotor organs of the Gyrinidae and other Coleoptera.

Li, M., Xi, N., Wang, Y. and Liu, L. (2019). Tunable Hybrid Biopolymeric Hydrogel Scaffolds Based on Atomic Force Microscopy Characterizations for Tissue Engineering. *IEEE Trans Nanobioscience* **18**, 597-610.

Martin, M. L., Travouillon, K. J., Fleming, P. A. and Warburton, N. M. J. J. o. m. (2020). Review of the methods used for calculating physiological cross‐sectional area (PCSA) for ecological questions. **281**, 778-789.

Ruan, Y., Konstantinov, A. S., Shi, G., Tao, Y., Li, Y., Johnson, A. J., Luo, X., Zhang, X., Zhang, M., Wu, J. et al. (2020). The jumping mechanism of flea beetles (Coleoptera, Chrysomelidae, Alticini), its application to bionics and preliminary design for a robotic jumping leg. *Zookeys* **915**, 87-105.

Saito, K., Nomura, S., Yamamoto, S., Niiyama, R. and Okabe, Y. (2017). Investigation of hindwing folding in ladybird beetles by artificial elytron transplantation and microcomputed tomography. *Proc Natl Acad Sci U S A* **114**, 5624-5628.

Saito, K. and Okabe, Y. (2015). Elastic wing deployments in beetles and their folding mechanisms. In *International Design Engineering Technical Conferences and Computers and Information in Engineering Conference*, vol. 57137, pp. V05BT08A033: American Society of Mechanical Engineers.

Sellers, K. C., Middleton, K. M., Davis, J. L. and Holliday, C. M. J. J. o. E. B. (2017). Ontogeny of bite force in a validated biomechanical model of the American alligator. **220**, 2036-2046.

Song, Z., Yan, Y., Tong, J. and Sun, J. (2020). Asian ladybird folding and unfolding of hind wing: biomechanical properties of resilin in affecting the tensile strength of the folding area. *Journal of Materials Science* **55**, 4524-4537.

Sutton, G. P. and Burrows, M. J. J. o. E. B. (2011). Biomechanics of jumping in the flea. **214**, 836-847.

Wan, C., Hao, Z. and Feng, X. J. S. r. (2016). Structures, properties, and energy-storage mechanisms of the semi-lunar process cuticles in locusts. **6**, 1-13.

Zhang, J., Yuan, Q., Jiang, Y., Pang, H., Rajabi, H., Wu, Z., Wu, J. J. B. and Biomimetics. (2021). Elytra coupling of the ladybird Coccinella septempunctata functions as an energy absorber in intentional falls. **16**, 056018.

Zhang, W., Li, M., Zheng, G., Guan, Z., Wu, J. and Wu, Z. (2020). Multifunctional mandibles of ants: Variation in gripping behavior facilitated by specific microstructures and kinematics. *J Insect Physiol* **120**, 103993.

Figures

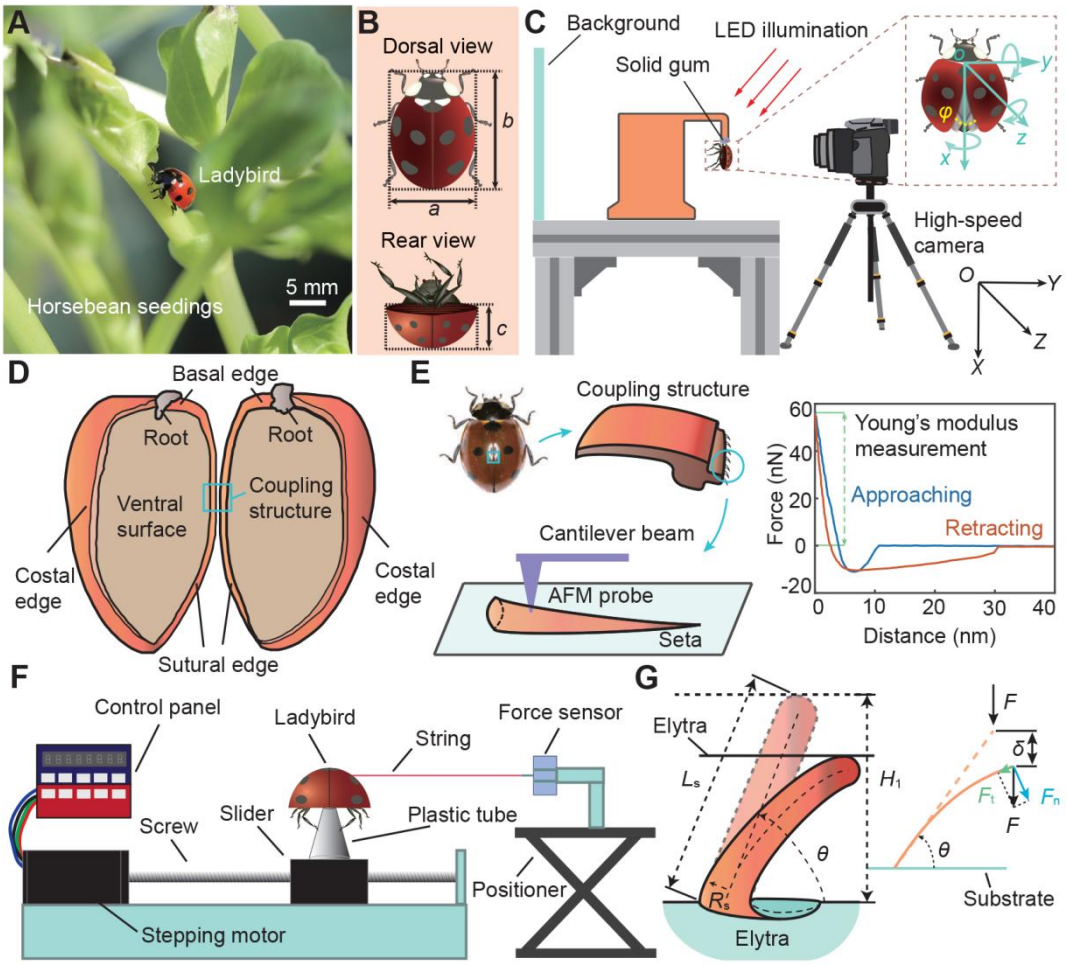

Fig. 1. Experimental techniques. (A) Ladybirds living in a cluster of horsebean seedings. (B) Dimensions of a ladybird body. (C) System for high-speed imaging of elytra opening in ladybirds. Schematic illustration of the *o-xyz* coordinates with the scutellum as the origin *o*. (D) Elytra viewed from below. (E) Schematic diagram of stiffness measurement of a seta using atomic force microscopy. (F) Experimental system to measure coupling forces between elytra. (G) Deflection of a seta under a load *F*.

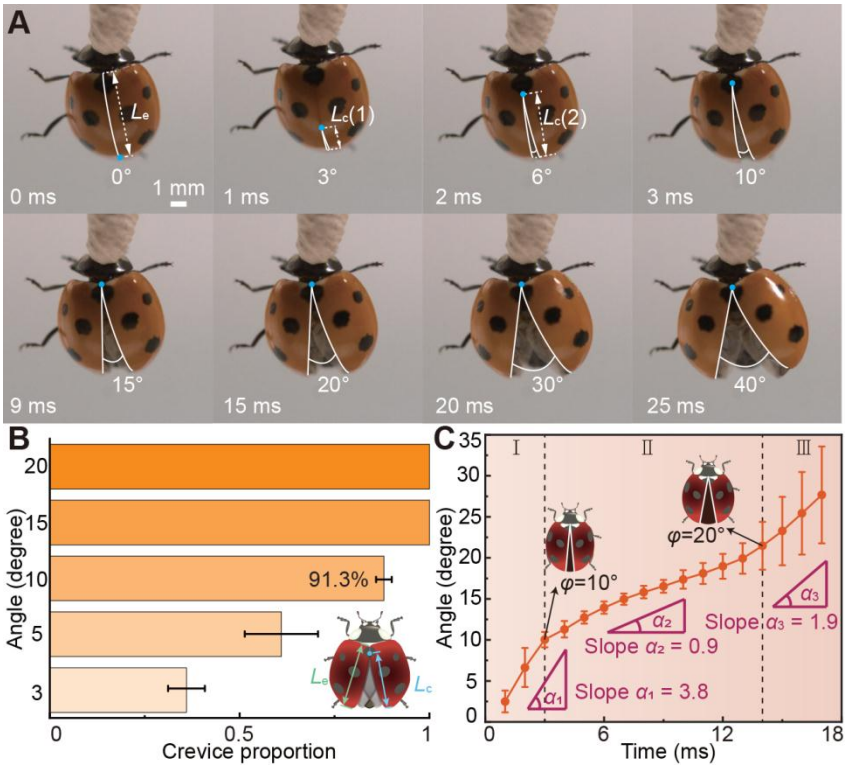

Fig. 2. Unfolding kinematics of a ladybird's elytra. (A) Snapshots of the elytra deployment. (B) Dynamic proportion of the crevice length L_c to the length of entire elytra L_e. (C) Splitting angle $\varphi(t)$ during elytra opening with the average angular velocity in the three phases described as slope α_1, slope α_2, and slope α_3, respectively. Transitions between the different phases are shown by the dotted lines.

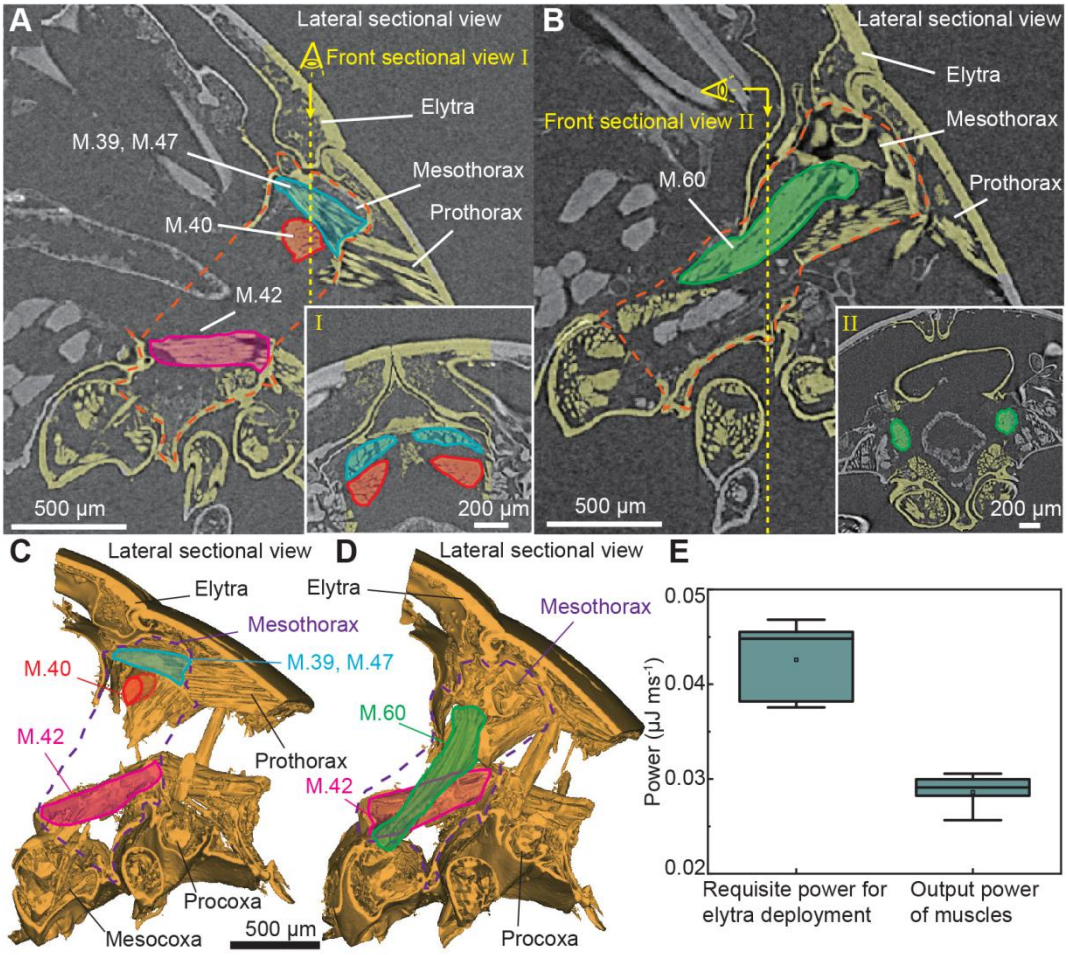

Fig. 3. Three-dimensional reconstruction of thoracic and sagittal section. (A-B) Sagittal section of thoracic muscles. Two typical front sectional views of muscles are shown in I and II. (A) Sagittal section of dorsal and ventral muscles. (B) Sagittal section of leg muscles. (C, D) 3D reconstruction of thoracic muscles based on serial sectioning. (E) Power required for elytra deployment (n = 10), and critical output power generated by elytral muscles (n = 4).

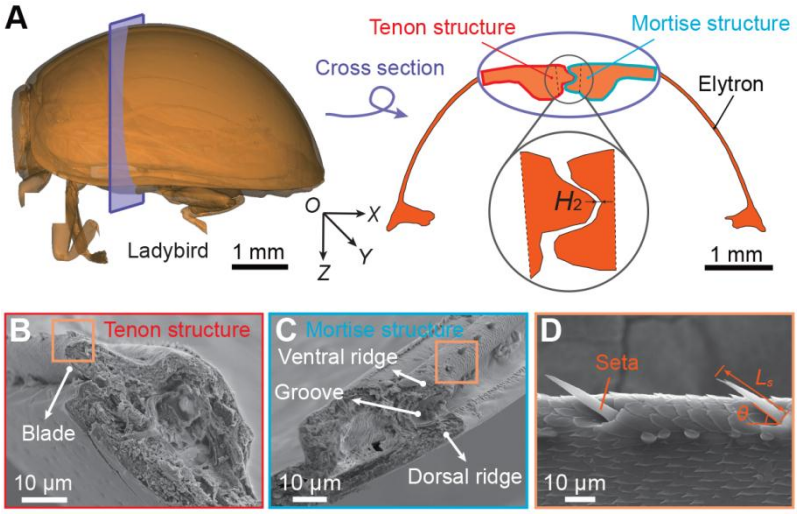

Fig. 4. Morphological features of the setae inside a ladybird beetle's elytra coupling. (A) Cross-section of a ladybird visualized by micro-CT scanning. (B, C) SEM images of the coupling structure of the elytra. Two rows of setae are arranged at the upper edge of the blade of tenon, and the upper edge of ventral ridge of mortise, respectively (orange squares). (D) SEM images showing seta.

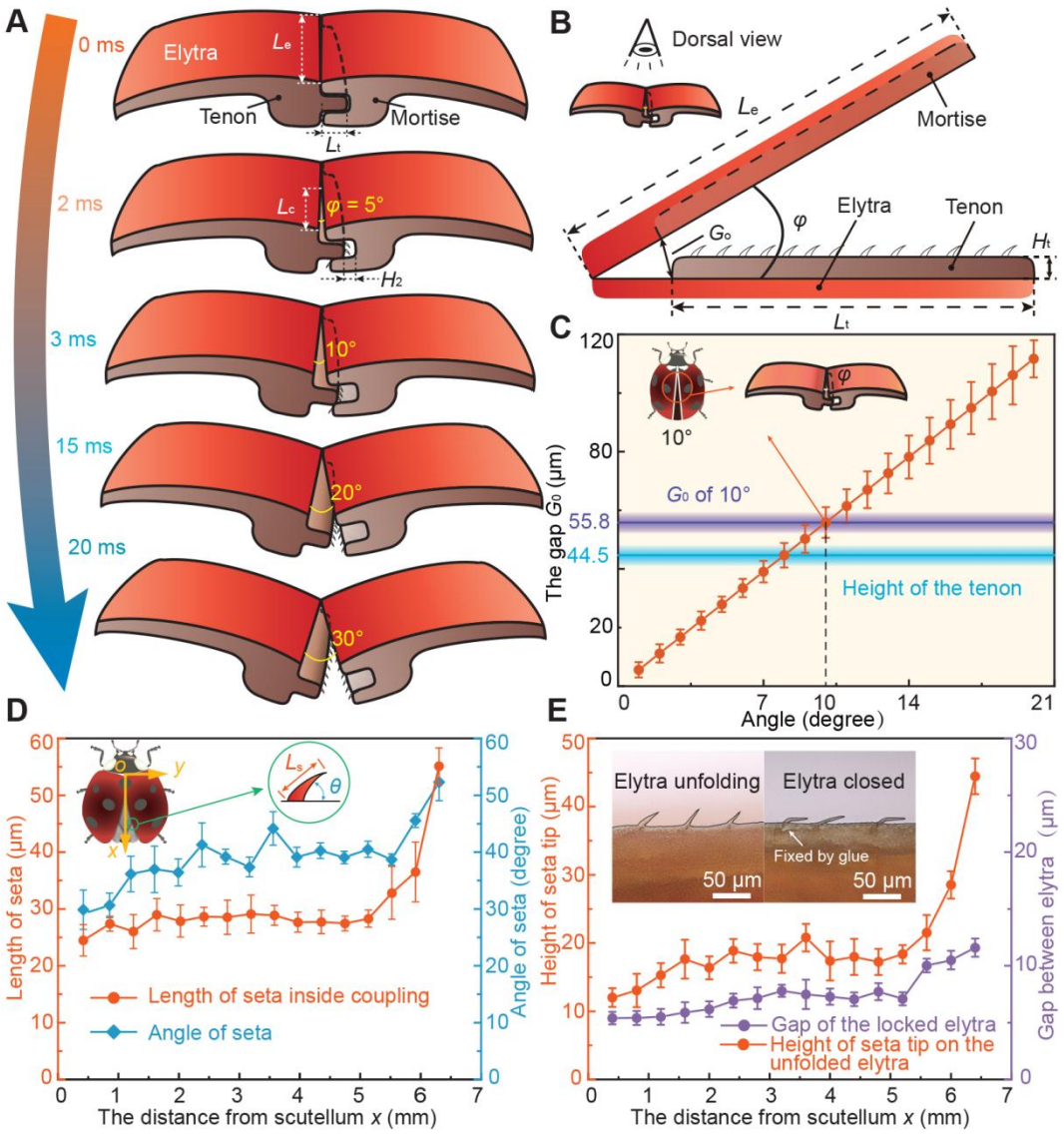

Fig. 5. Effect of elytra closing on seta shape. (A) Changes in configuration of tenon and mortise structures during elytra deployment. (B) Schematic illustration of the deployment of elytra (dorsal view). (C) Initial gap between elytra G_0 as a function of position along the tenon prior to elytra unfolding. (D) Geometry of setae. The coordinate system uses the scutellum as the origin *o*. The *x* axis originates from point *o* and extends posteriorly, the *y* axis is perpendicular to the *x* axis. (E) Height of setae and width of the gap between elytra as a function of distance from the scutellum. Fixed setae were visualized by injection of glue into the coupling structure of the closed elytra.

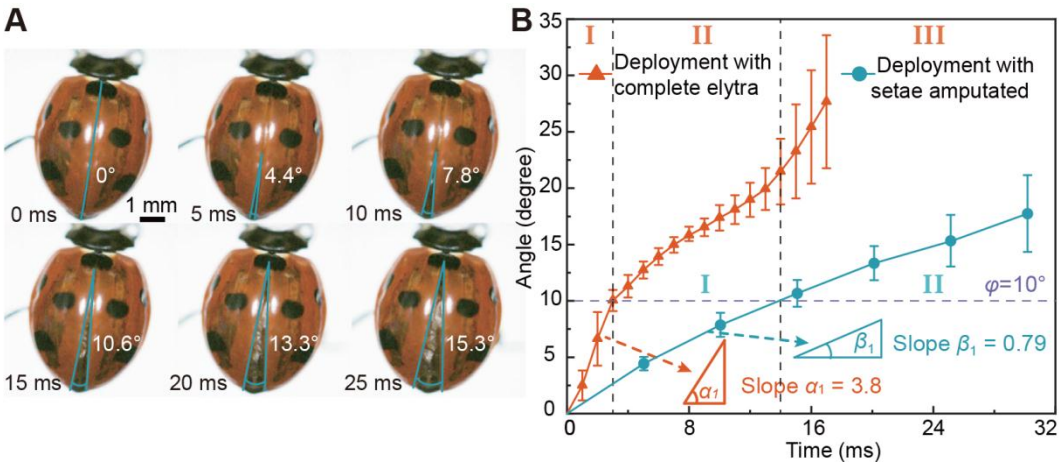

Fig. 6. Kinematics of elytra deployment with coupling setae removed. (A) Snapshots of the initial phase of the elytra deployment with setae removed. (B) Angle φ and angular velocity ω of elytra during elytra opening. The angular velocities of the intact elytra and setae-excised elytra in the initial phases are depicted as the slopes α_1 and β_1, respectively.

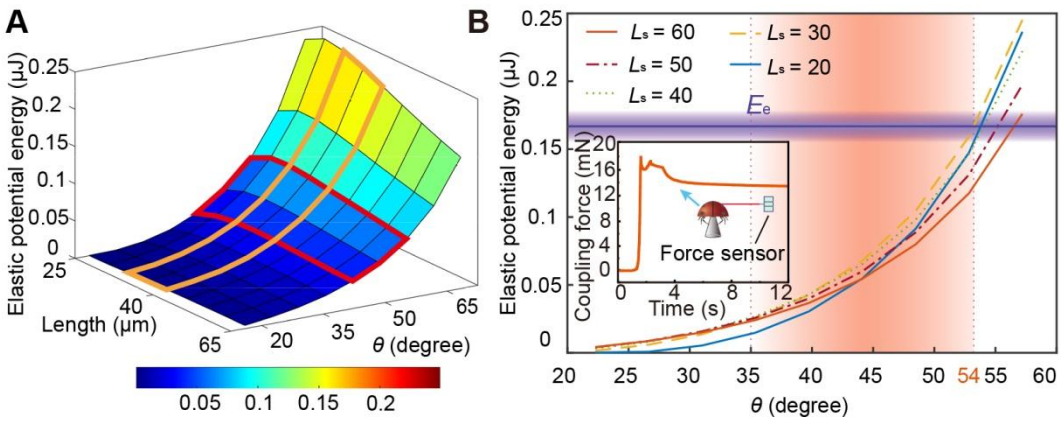

Fig. 7. Effects of morphological geometry of setae on elastic energy storage. (A) Elastic potential energy of setae E_s related to setae length and angle. The regions outlined in orange and red indicate ranges of the setae length and angles captured from experiments. (B) Coupling force F_c and elastic energy E_s stored in setae for different angles. Pink shaded area suggests preferred angles ($35 < \theta < 54$) that can satisfy a trade-off between swiftness of elytra opening and stability of elytra locking.

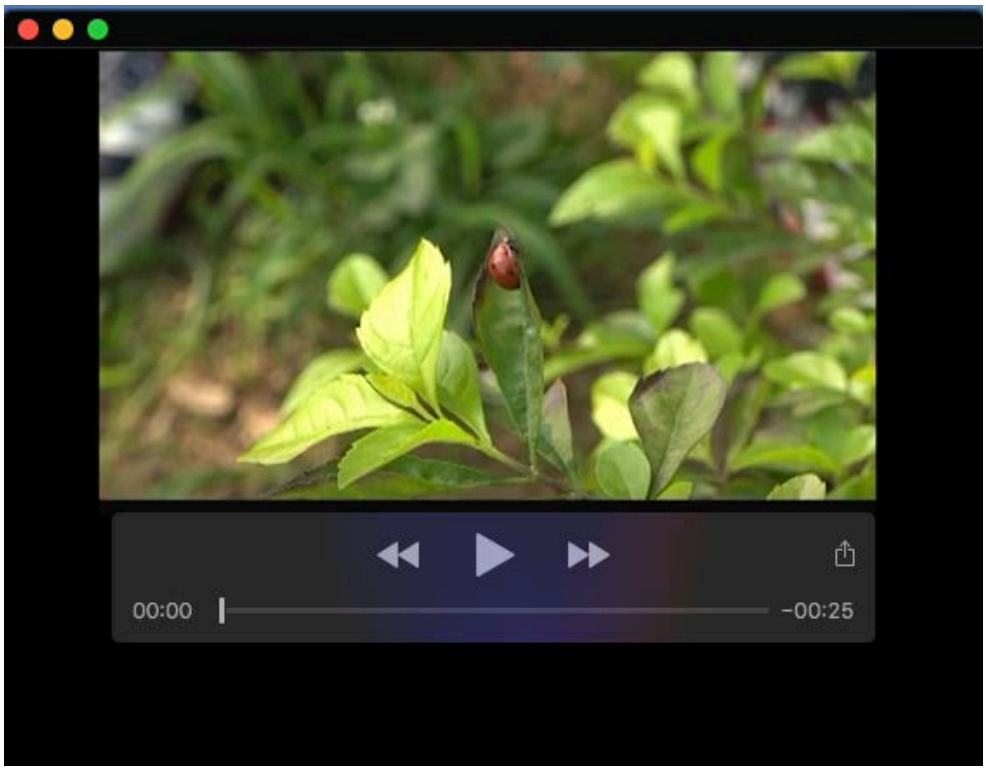

Movie 1. Elytra deployment of a living ladybird.

Movie 2. Sagittal section thoracic muscles of a ladybird.

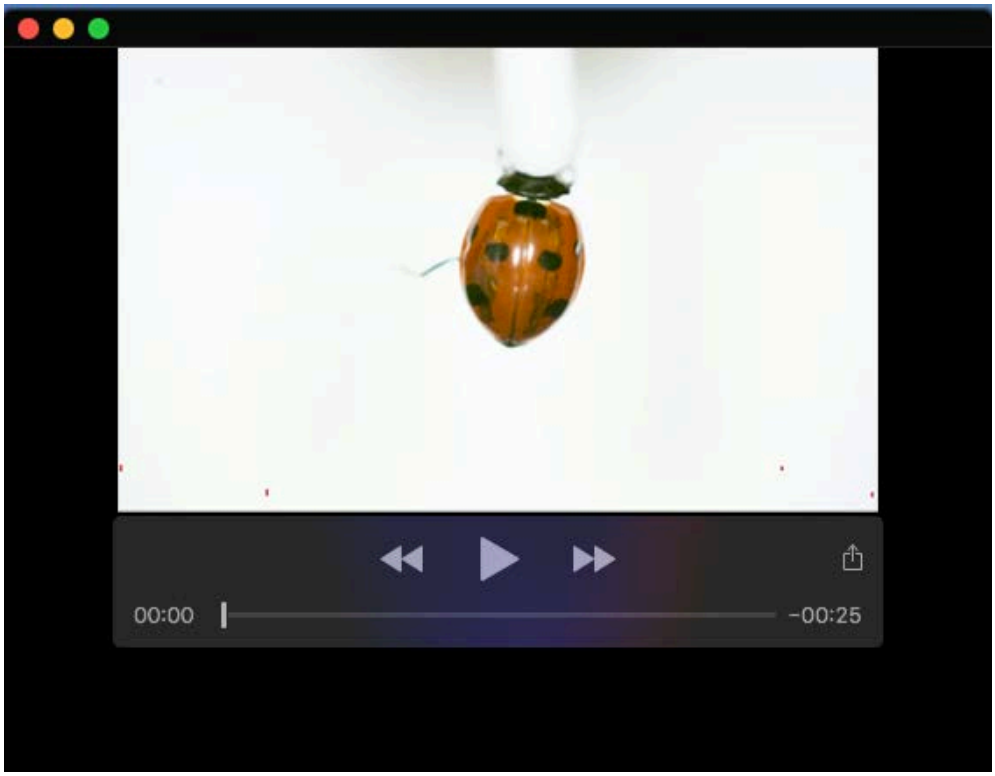

Movie 3. Deployment of a ladybird elytra with setae scraped off.